In-Depth Lab Report

Laboratory Evaluation of Angle Grinder Discs for Grinding and Cutting Engineered Stone

Drew Thompson, PhD

Esther Ku

Chaolong Qi, PhD, PE

Commander, U.S. Public Health Service

Division of Field Studies and Engineering
Engineering and Physical Hazards Branch
EPHB Report No. 2025-DFSE-2042
May, 2025

Disclaimer

The findings and conclusions in this report are those of the author(s) and do not necessarily represent the official position of the National Institute for Occupational Safety and Health (NIOSH), Centers for Disease Control and Prevention (CDC). Mention of any company or product does not constitute endorsement by NIOSH/CDC.

In addition, citations to websites external to NIOSH do not constitute NIOSH endorsement of the sponsoring organizations or their programs or products. Furthermore, NIOSH is not responsible for the content of these websites. All Web addresses referenced in this document were accessible as of the publication date.

Table of Contents

Abstract

Background

Workplace exposure to respirable crystalline silica (RCS) can cause silicosis, a progressive lung disease marked by scarring and thickening of the lung tissue. Crystalline silica is found in several materials, such as brick, block, mortar, and concrete. Construction and manufacturing tasks that cut, break, grind, abrade, or drill those materials have been associated with overexposure to dust containing RCS. Stone countertop products can contain various levels of crystalline silica (can be >90 wt%) and working with this material during stone countertop fabrication has been shown to cause excessive RCS exposures. NIOSH scientists conducted a study to develop a control strategy for workers' RCS exposure during stone countertop fabrication. The laboratory research described in this report is part of that study.

Assessment

NIOSH scientists systematically characterized the airborne dust generated from grinding and cutting an engineered stone product using a laboratory testing system designed and operated to collect representative respirable dust samples. The laboratory experiments in this study determined crystalline silica content, respirable dust and RCS generation rates, and dust size distributions during dry grinding using an angle grinder with fine, medium, and coarse grit grinding cup wheels and during dry cutting with a cutting blade.

Results

There was no statistically significant difference in the mean crystalline silica content of the respirable dust generated by each angle grinder disc. The mean normalized generation rates of respirable dust and RCS were highest for the fine grit grinding cup wheel, followed in decreasing order by the medium grit grinding cup wheel, the coarse grit grinding cup wheel, and, finally, the cutting blade. The operation of the cutting blade and all grinding cup wheels generated mass-based size distributions with their most prominent mode located at an aerodynamic diameter of about 4.7 – 6.8 μm, with the mode increasing in size with increasing grit coarseness for the grinding cup wheels and being highest for the cutting blade.

Conclusions and Recommendations

When removing the same volume of engineered stone by grinding or cutting activities, workers are likely to be exposed to lower quantities of RCS when cutting with a cutting blade, followed by grinding with a coarse grit grinding cup wheel, then grinding with a medium grit grinding cup wheel, and, finally, grinding with a fine grit grinding cup wheel. This suggests that an appropriate administrative control could be to train workers to prioritize cutting over grinding, when feasible, and when grinding prioritize grinding cup wheels with coarser grits whenever suitable for the surface finish required. This approach likely aligns with the workflow

already used by most stone countertop fabricators, as it also maximizes the workpiece removal rate–a measure of process productivity.

Introduction

Background for Control Technology Studies

The National Institute for Occupational Safety and Health (NIOSH) is the primary Federal agency engaged in occupational safety and health research. Located in the Department of Health and Human Services, it was established by the Occupational Safety and Health Act of 1970. This legislation mandated NIOSH to conduct a number of research and education programs separate from the standard setting and enforcement functions carried out by the Occupational Safety and Health Administration (OSHA) in the Department of Labor. An important area of NIOSH research deals with methods for controlling occupational exposure to potential chemical and physical hazards. The Engineering and Physical Hazards Branch (EPHB) of the Division of Field Studies and Engineering has been given the lead within NIOSH to study the engineering aspects of health hazard prevention and control.

Since 1976, EPHB has conducted assessments of health hazard control technologies on the basis of industry, common industrial processes, or specific control techniques. Examples of these completed studies include the foundry industry; various chemical manufacturing or processing operations; spray painting; and the recirculation of exhaust air. The objective of each of these studies has been to document and evaluate effective control techniques for potential health hazards in the industry or process of interest, and to create a more general awareness of the need for, or availability of, an effective system of hazard control.

These studies involve a number of steps or phases. Initially, a series of walk-through surveys is conducted to select plants or processes with effective and potentially transferable control concept techniques. Next, in-depth laboratory studies and/or field surveys are conducted to determine both the control parameters and the effectiveness of these controls. The reports from these in-depth studies are then used as a basis for preparing technical reports and journal articles on effective hazard control measures. Ultimately, the information from these research activities builds the data base of publicly available information on hazard control techniques for use by health professionals who are responsible for preventing occupational illness and injury.

Background for this Project

Crystalline silica refers to a group of minerals composed of silicon and oxygen; a crystalline structure is one in which the atoms are arranged in a repeating three-dimensional pattern [Bureau of Mines, 1992]. The three major forms of crystalline silica are quartz, cristobalite, and tridymite; quartz is the most common form [Bureau of Mines, 1992]. Respirable crystalline silica (RCS) refers to that portion of airborne crystalline silica dust that is capable of entering the gas-exchange regions of the lungs if inhaled; this includes particles with aerodynamic diameters less than approximately 10 micrometers (μm) [NIOSH, 2002]. Silicosis, a fibrotic disease of the lungs, is an occupational respiratory disease caused by the inhalation and

deposition of RCS dust [NIOSH, 1986]. Silicosis is irreversible, often progressive (even after exposure has ceased), and potentially fatal. Because no effective treatment exists for silicosis, prevention through exposure control is essential.

Stone countertops have become increasingly popular among consumers in recent years. Granite and engineered quartz stone are the two major stone countertop materials, respectively representing an estimated 27% and 8% market share (by sales) in a $74B global countertop market in 2012. Rose et al. [2019] reported that there were an estimated 8,694 establishments and 96,366 employees in the stone fabrication industry in the United States in 2018 by analyzing data from the Bureau of Labor Statistics.

Unfortunately, a large amount of dust that contains RCS can be produced during stone countertop fabrication and installation. On average, granite naturally contains 72% crystalline silica by weight [Blatt and Tracy, 1997], and engineered quartz stone contains about 90% quartz grains by mass in a polymer matrix [Phillips et al., 2013]. An outbreak of silicosis was reported in Israel [Kramer et al., 2012], where 25 patients were identified who shared an exposure history of having worked with engineered quartz stone countertops without dust control or respiratory protection. In addition, 46 silicosis cases were reported in Spain among men working in the stone countertop cutting, shaping, and finishing industry [Pérez-Alonso et al., 2014] In 2015, the first silicosis case in the US was reported for a worker who had worked with engineered quartz stone countertops [Friedman et al., 2015]; and NIOSH and OSHA [2015] released a Hazard Alert on worker exposure to silica during countertop manufacturing, finishing and installation. More recently, Rose et al. [2019] reported 18 silicosis cases, including two fatalities, among workers in the stone fabrication industry in California, Colorado, Texas, and Washington of the US; and Fazio et al. [2023] reported 52 silicosis cases, including 10 fatalities, in the state of California. A systematic evaluation, optimization, and improvement of exposure control measures for processes involved in stone countertop fabrication and installation would help give manufacturers, fabricators, and occupational safety and health professionals best-practice recommendations for consistently reducing RCS exposures below the NIOSH Recommended Exposure Limit (REL) of 0.05 mg/m^3 (50 $\mu g/m^3$).

A review of workplace inspections conducted by the state of Washington's Department of Labor and Industries found overexposures to RCS (above the OSHA Permissible Exposure Limit (PEL)) and violation of rules on engineering controls in 9 of 18 stone countertop shops inspected [Lofgren, 2008]. Data from OSHA's Integrated Management Information System (IMIS) reveals that citations issued for exceeding the PEL for RCS jumped from an average of 4 per year during 2000-2002 to an average of 59 per year during 2003-2011 at stone countertop fabrication shops and installation sites. These results indicate that dust control methods did not appear to be well implemented among shops in this industry. OSHA published a new PEL of 0.05 mg/m^3 (50 $\mu g/m^3$) as an 8-hr time weighted average (TWA) for RCS [81 Fed. Reg. 16285, 2016], making it critical to address these overexposures.

This project aims at reducing workers' exposures and risks in the stone countertop fabrication and installation industries by evaluating, optimizing, and improving exposure control measures, evaluating their effectiveness through in-depth laboratory and field studies, and disseminating the results through NIOSH field survey reports, articles in professional and trade journals, and a NIOSH Internet topic page. The long-term objective of this study is to provide practical recommendations for effective dust controls that will prevent overexposures to RCS during stone countertop fabrication and installation.

Background for this Study

In a survey of 47 granite countertop fabrication shops in Oklahoma, 15% of shops reported using dry methods for edge grinding most of the time [Phillips and Johnson, 2012]. This value is similar to the findings of Glass et al. [2022] where 16% of the 324 participants in the engineered stone fabrication industry in Victoria, Australia spent more than 50% of the time doing dry work in their most recent jobs. Field studies by NIOSH [NIOSH, 2016a; NIOSH, 2016b; NIOSH, 2016c] in relatively large stone countertop fabrication shops found that cutting was mostly performed by machines operated remotely, such as bridge saws or water-jet cutters, but final grinding of the stone edge profiles was exclusively conducted by workers using hand-held grinders. Those grinding tasks led to the highest RCS exposure among workers in these shops. The NIOSH studies reported overexposure to RCS for the workers conducting grinding and some polishing tasks in these shops, even when regular wet methods were employed. A recent NIOSH study [2021] reported that the RCS exposure for workers conducting grinding tasks can be reduced to levels below the OSHA PEL by supplementing the regular wet methods incorporated in the grinders with a sheet-water-wetting method. Additional or more effective exposure controls could consistently reduce RCS exposures to permissible levels.

When developing effective and feasible exposure controls, dust and crystalline silica generation rates, dust size distribution, and crystalline silica content are valuable information [Qi et al., 2016]. This characterization is best done systematically in a well-controlled laboratory test system. As part of this project, such a system was used in a prior NIOSH study to characterize the dust emissions from dry grinding natural and engineered stone products to (i) identify stone products currently available that potentially lower or eliminate RCS exposure (via substitution or elimination) and (ii) aid the development and/or implementation of potential engineering control measures [NIOSH, 2023]. Elimination, substitution, and engineering controls are the most effective exposure control methods because they reduce risks without requiring much action from workers. They can be combined with administrative controls, which establish work practices that also help lower exposures to hazards. If certain angle grinder discs were found to generate less RCS, one possible administrative control could be to train countertop fabricators to prioritize the use of angle grinder discs which would minimize potential RCS exposures. Therefore, this study was designed to characterize the dust generated from engineered stone during dry grinding with fine, medium, and coarse grit grinding cup wheels and during dry cutting with a cutting blade inside a controlled

laboratory testing system following standard methods to determine dust and crystalline silica generation rates, dust size distributions, and crystalline silica content. The results will serve as the basis to evaluate potential administrative control effectiveness by comparing generation rates obtained from the same standard method.

Materials and Methods

Laboratory Testing System

The laboratory testing system used in this study was designed and operated to comply with European Standard EN 1093-3 [CEN, 2006] and is shown in Figure 1. The system consisted of an enclosed chamber where the airborne dust was generated, a funnel, and a measurement duct where the airborne dust was sampled. A house ventilation system equipped with a variable-speed blower drew room air into the test system through pre- and HEPA filters at a flow rate of 0.17 $m^3\ s^{-1}$. The flow rate was monitored by a micromanometer (Airflow™ MEDM 500, Airflow Developments LTD., UK) connected to a delta tube (306AM-11-AO, Midwest instruments, USA) which functioned as an averaging pitot tube. Under the operating flow rate used in this study, the average flow velocity in the chamber was 0.11 m s^{-1} which meets the standard's requirement that it be greater than or equal to 0.1 m s^{-1} for the transport of respirable dust. The Reynolds numbers for the chamber and measurement duct were 9,100 and 46,000, respectfully, indicating that the flow was turbulent. Turbulent flow causes aerosol mixing and allows for the collection of representative samples in the measurement duct. After the measurement duct, air was passed through the filter cartridges inside an air handling unit (PSKB-1440, ProVent LLC, USA) that was not driving airflow before discharging into the house ventilation duct.

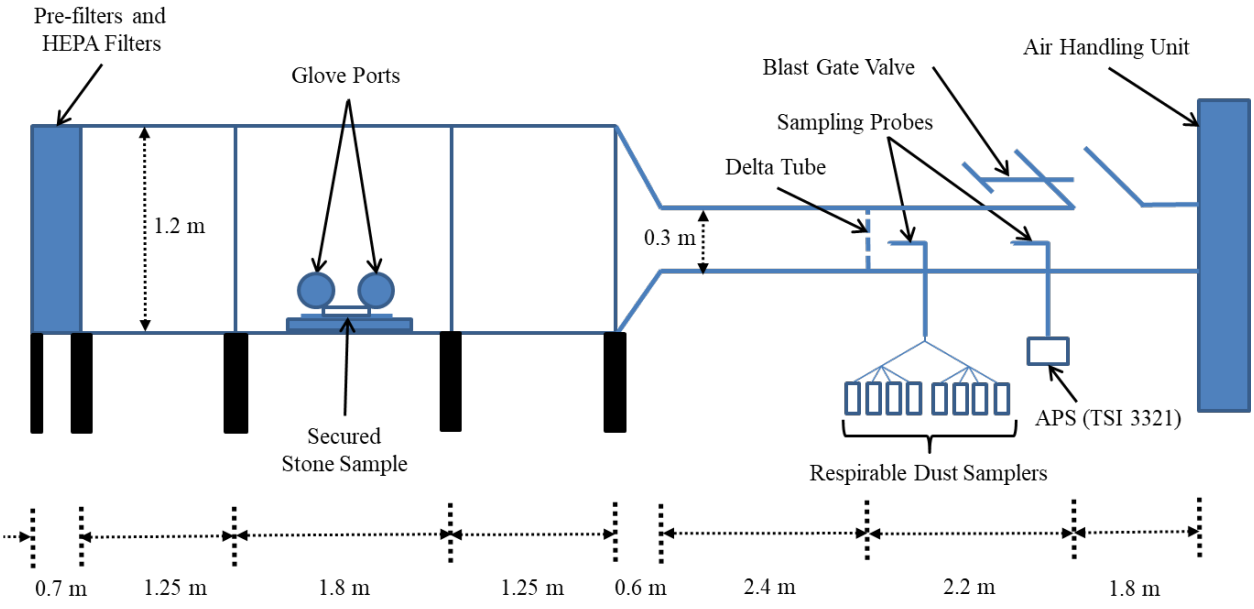

Figure 1. Diagram of the laboratory testing system

Test Conditions

The workpiece in this study was an engineered stone product containing 70-90% crystalline silica in a polymer resin matrix. The manufacturer reported composition, sample dimensions, and measured material density for the engineered stone product are listed in Table 1.

Table 1. Summary of engineered stone product properties

Manufacturer crystalline silica content (%)	Thickness (mm)	Material density, ρ_m (kg m^{-3})
70-90	19	2100

A pneumatic angle grinder (GPW-216, Gison Machinery Co., Ltd., Taiwan) was manually operated through the chamber's glove ports. Four discs were tested: three grinding cup wheels with different abrasive grits and one cutting blade. Three diamond grinding cup wheels with fine, medium, and coarse abrasive grits were used to grind the edge of the workpiece. A diamond cutting blade was used to cut grooves along the width of the workpiece. The angle grinder disc descriptions, model numbers, and manufacturers are listed in Table 2.

Table 2. Summary of angle grinder discs

Disc label	Description	Model	Manufacturer
Fine	10 cm diameter, fine abrasive grit, diamond grinding cup wheel	SIS-4SPCW-SF	Stone Industrial Supplies, Inc.
Medium	10 cm diameter, medium abrasive grit, diamond grinding cup wheel	SIS-4SPCW-SM	Stone Industrial Supplies, Inc.
Coarse	10 cm diameter, coarse abrasive grit, diamond grinding cup wheel	SIS-4SPCW-SC	Stone Industrial Supplies, Inc.
Cutting	13 cm diameter, diamond, dry cutting, granite turbo blade	SIS-S5G	Stone Industrial Supplies, Inc.

We conducted three experimental runs for each disc. For the three grinding cup wheels, one operator ground the stone sample continuously for 4 min in each experimental run. For the cutting blade, one operator cut multiple grooves in the stone sample. The estimated duration of the cutting task varied from 2.5 to 4 minutes for each experimental run. Before and after each experimental run, the workpiece was weighed on a scale with 2 g certified readability (Model D51XW10WR3, OHAUS Corp., USA) to determine the mass of swarf (i.e., stone fragments and dust) removed during the task. A material removal rate was calculated from the swarf mass removed, material density, and duration of the task.

Sampling Methods

Two isoaxial sampling probes extracted aerosols from the measurement duct of the testing system to (a) eight respirable dust samplers operated in parallel and (b) an Aerodynamic Particle Sizer (APS) Spectrometer (Model 3321, TSI Inc., USA). The sampling probes were near-isokinetic and estimated to have less than 10% sampling bias for particles smaller than 11 µm by following Brockmann [2011]. Probes were connected to their respective samplers and instrumentation using metallic fittings and Tygon® or conductive silicone tubing to minimize particle losses caused by electrostatic effects. The respirable dust sampler aerosol flow was split by first passing through a wye fitting followed by a 4-way flow splitter (Model 3708, TSI Inc., USA) on both branches. The overall sampling biases of the sampling trains were estimated to be less than 10% for particles with diameters ranging from 5 nm to 9 µm [Thompson and Qi, 2023].

GK 4.162 RASCAL Cyclones (Mesa Laboratories, Inc., USA) operated at a flow rate of 9.0 l min^{-1} were used to collect respirable dust on 47 mm diameter, 5 µm pore size, polyvinyl chloride (PVC) filters backed by cellulose support pads in three-piece conductive cassettes following NIOSH Methods 0600 and 7500 [NIOSH, 1998; NIOSH, 2003]. The sampling flow rates for the respirable samplers were provided by Leland Legacy Sample Pumps (SKC Inc., USA).

PVC filters were pre-weighed and post-weighed to determine respirable dust mass collected. Crystalline silica analysis of each air sample was performed by x-ray diffraction (XRD) in accordance with NIOSH Method 7500 [NIOSH, 2003] to quantify the amount of quartz, cristobalite, and tridymite forms of crystalline silica present. The PVC filters from all the air samples were processed by muffle furnace ashing for sample preparation to avoid the potential underestimation of crystalline silica caused by dissolution of engineered stone dust samples in tetrahydrofuran (THF) [Qi et al., 2022]. Limits of detection (LOD) for each analyte were as listed in Table 3 and depended on analytical instruments, analysts, and XRD interferences. Limits of quantification (LOQ) were calculated as 10/3 times the LOD.

Table 3. Limits of detection (LOD) for the analysis of air samples

	Respirable dust	Cristobalite	Quartz	Tridymite
LOD (µg $sample^{-1}$)	18 or 36	5	5	10 or 20
LOQ (µg $sample^{-1}$)	61 or 120	17	17	33 or 67

From the mass of the dust and crystalline silica of each sample, we calculated the crystalline silica content and the normalized generation rate. Crystalline silica content was defined as the percent crystalline silica by weight. The normalized generation rate, G, represented the mass of airborne respirable dust or RCS generated per unit of swarf volume removed from the workpiece and is defined by Equation 1, where ρ_m is the bulk material density of the stone sample, m_{sampl} is the mass collected by the respirable sampler, m_{remov} is the swarf mass removed from

the stone sample, and Q and Q_{sampl} are the nominal flow rates of the test chamber and respirable sampler, respectively.

$$G = \frac{Q\rho_m m_{sampl}}{Q_{sampl} m_{remov}} \quad \textbf{Equation 1}$$

Crystalline silica content and normalized generation rate are not measured directly, but instead determined through other quantities via functional relationships. Thus, the combined standard uncertainty for uncorrelated input quantities, as defined in Equation 2, was used to estimate the standard deviation by following the approach of the International Organization for Standardization [2008]:

$$u_c(y) = \sqrt{\sum_{i=1}^{N} \left(\frac{\partial f}{\partial x_i}\right) u^2(x_i)} \quad \textbf{Equation 2}$$

where f is the functional relationship, x_i is the arithmetic mean of mass measurement i (dust, quartz, cristobalite, or tridymite), $u(x_i)$ is the standard uncertainty of mass measurement i, N is the number of mass measurements, and $\partial f/\partial x_i$ is evaluated at x_i.

We performed Welch's analysis of variance (ANOVA) for hypothesis testing to determine whether the crystalline silica content, respirable dust normalized generation rates, RCS normalized generation rates, and material removal rates for each angle grinder disc had equal means. In the calculation of p-values, we used combined standard uncertainty calculated from Equation 2 as an estimate of standard deviation, when appropriate. The null hypothesis was rejected for p-values less than 0.05.

The size distributions of particles with aerodynamic diameters ranging from 0.5 to 20 µm were measured every 1 s by the APS. A correction was applied in the Aerosol Instrument Manager (AIM) (v10.2.0.11, TSI Inc., USA) software package to improve APS sizing accuracy for particles with densities that aren't close to unit density, 1000 ± 100 kg m^{-3} [Wang and John, 1987; TSI Incorporated, 2013]. See Appendix I for more details. Number and mass-based particle size distributions representative of the stone grinding or cutting process were obtained from the APS. To account for transients due to particle transport in the testing system, the periods of active grinding and cutting were identified as those having the highest moving average of particle number concentration over the nominal task duration. In the case of stone cutting, the nominal task duration was estimated to the nearest 0.5 min. For each angle grinder disc, the particle number and mass distributions were calculated from the APS data collected each second during periods of active grinding or cutting. Multimodal lognormal size distribution functions were fit to APS-measured particle number distributions following the procedure outlined in Appendix I.

Results

Crystalline Silica Content in Respirable Dust Samples

Respirable dust samples from all angle grinder discs contained cristobalite (44 – 47 wt%) and quartz (19 – 21 wt%) forms of crystalline silica but no tridymite. The crystalline silica content by percent mass in respirable dust is presented in Figure 2 (see Table 7 in Appendix III for the tabulated data in this figure, in addition to the combined standard uncertainties of cristobalite and quartz content) and ranged from 63 to 68 wt%. There was no statistically significant difference between the mean crystalline silica content of the respirable dust generated by each angle grinder disc (p = 0.78).

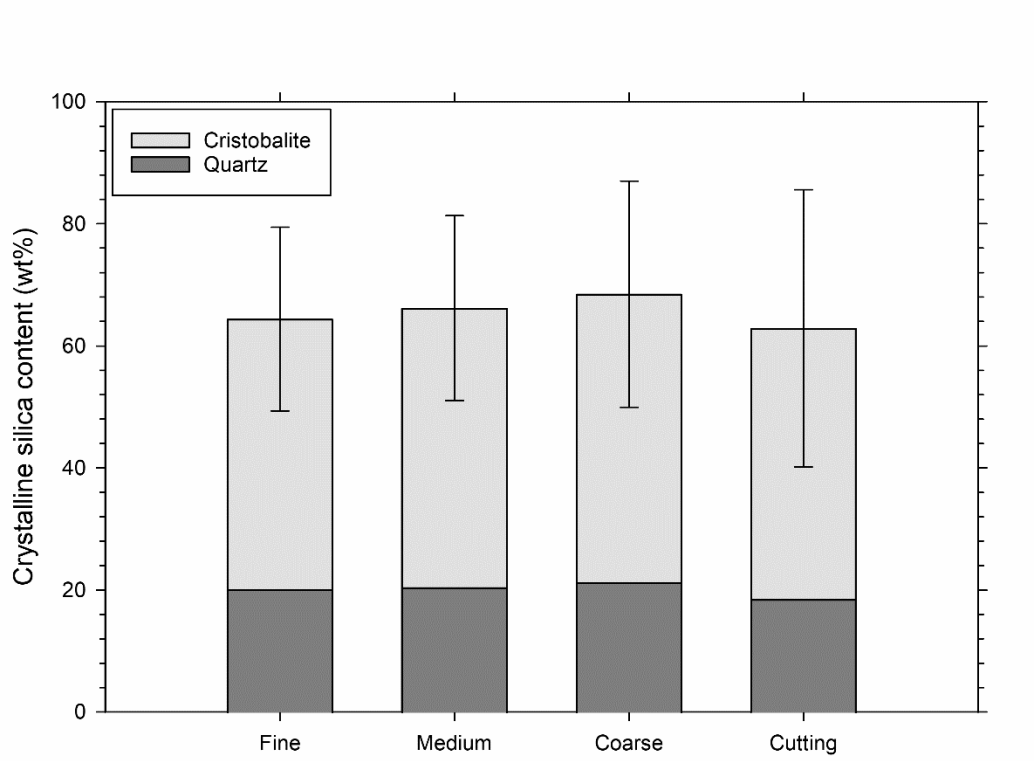

Figure 2. Crystalline silica content of respirable dust. Shadings represent the fraction of cristobalite and quartz forms. Error bars represent the combined standard uncertainty of crystalline silica content.

Respirable Dust and Crystalline Silica Normalized Generation Rates

The mean normalized generation rates of respirable dust and RCS from grinding engineered stone with fine, medium, and coarse grit grinding cup wheels and cutting it with a cutting blade are plotted in Figure 3. The mean normalized generation rates of respirable dust and RCS ranged from 15 to 38 mg cm^{-3} and 9.4 to 24 mg cm^{-3}, respectively. Both generation rates were highest for the fine grit grinding cup wheel, followed in decreasing order by the medium grit grinding cup wheel, the coarse grit grinding cup wheel, and, finally, the cutting blade. There was

a statistically significant difference in the mean normalized generation rates of respirable dust (p = 6.9E-18) and RCS (p = 1.0E-16) for each angle grinder disc.

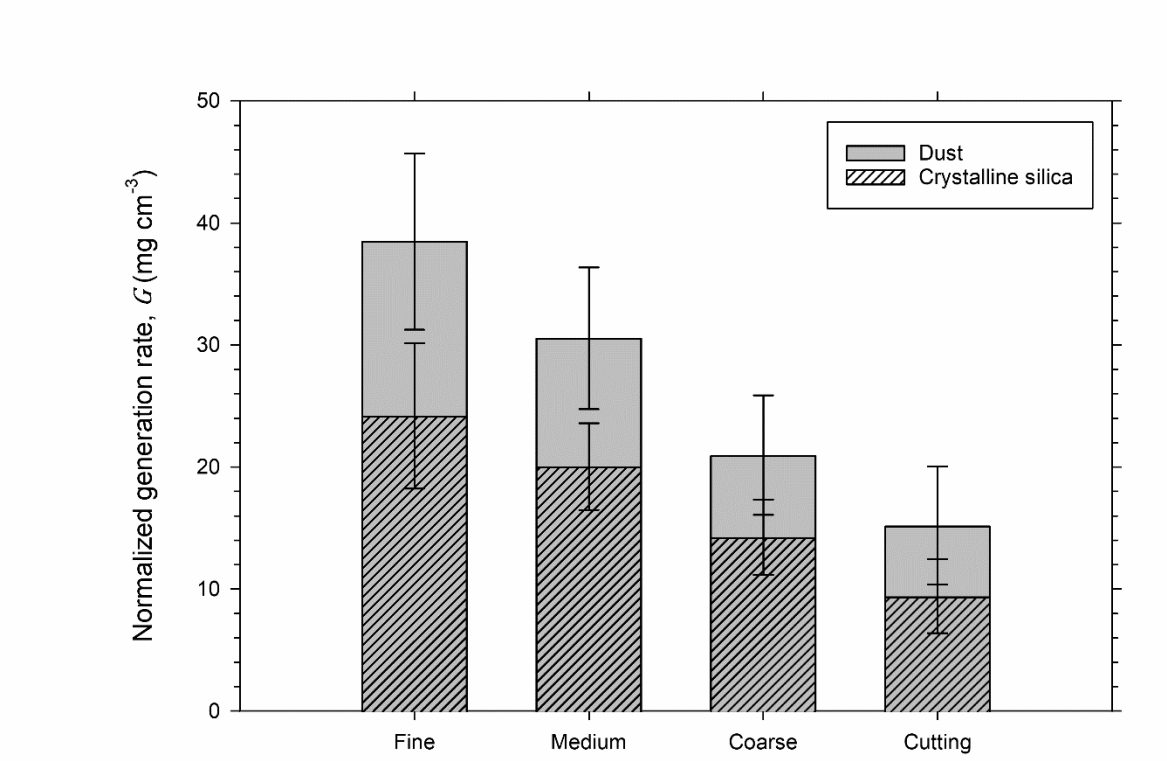

Figure 3. Respirable dust and RCS normalized generation rates. Each datum represents the mass of dust or crystalline silica (units of mg) normalized by the volume removed from the stone sample during grinding or cutting (units of cm^3). Error bars represent the combined standard uncertainty of the normalized generation rate.

Material Removal Rates

Mean material removal rates from the grinding and cutting of engineered stone are shown in Figure 4. The mean material removal rates ranged from 5.0 to 9.2 cm^3 min^{-1} and were ranked, in decreasing order: coarse grit grinding cup wheel, medium grit grinding cup wheel, cutting blade, and fine grinding cup wheel. There was a statistically significant difference in the mean material removal rates (p = 0.0054) for each angle grinder disc.

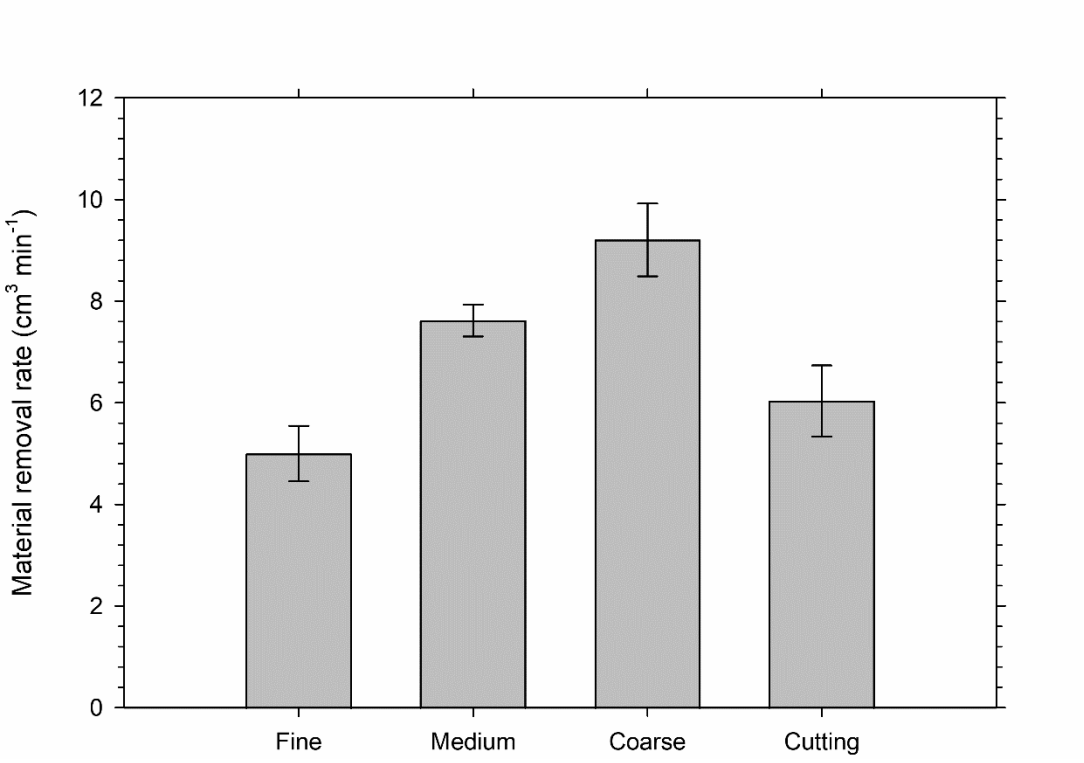

Figure 4. Material removal rate from three experimental runs of grinding or cutting engineered stone. Error bars represent the standard deviation of three replicates.

Particle Size Distributions

The number-based and mass-based particle size distributions measured by APS, and corrected to account for particle density and shape, during the grinding or cutting of engineered stone are plotted in Figure 5. Plotted along with the APS data are the best fit multimodal lognormal distributions (see Table 4 in Appendix I for the best fit, number-based, multimodal lognormal distribution parameters). The total number concentration was highest during grinding with the medium grit grinding cup wheel, followed in decreasing order by the fine grit grinding cup wheel, the coarse grit grinding cup wheel, and the cutting blade. In the number-based size distributions, all angle grinder discs produced size distributions that had their most prominent mode located at an aerodynamic diameter of about 2.2 – 2.4 µm, second most prominent mode at 0.77 – 0.93 µm, and third most prominent mode at 6.4 – 6.9 µm. In addition, the size distribution generated by the cutting blade had a fourth and least prominent mode at 18 µm. The multimodal lognormal distributions exhibited an excellent fit with coefficients of determination, R^2, greater than 0.99 for all discs.

The total mass concentration was highest during grinding with the medium grit grinding cup wheel, followed in decreasing order by the coarse grit grinding cup wheel, the fine grit grinding cup wheel, and the cutting blade. Following the methodology outlined in Appendix I to derive mass-based distributions from the best fit number-based size distributions, we see the most prominent modes at 4.7 –

6.8 µm in the mass-based particle size distributions, as shown in Figure 5(b) (see Table 5 in Appendix I for the derived mass-based, multimodal lognormal distribution parameters). The most prominent modes of the mass-based particle size distributions increased with increasing grit coarseness for the grinding cup wheels and was highest for the cutting blade. The aerodynamic diameters for these modes were 4.7 µm, 5.0 µm, 5.4 µm, and 6.8 µm for the fine grit grinding cup wheel, medium grit grinding cup wheel, coarse grit grinding cup wheel, and cutting blade, respectively.

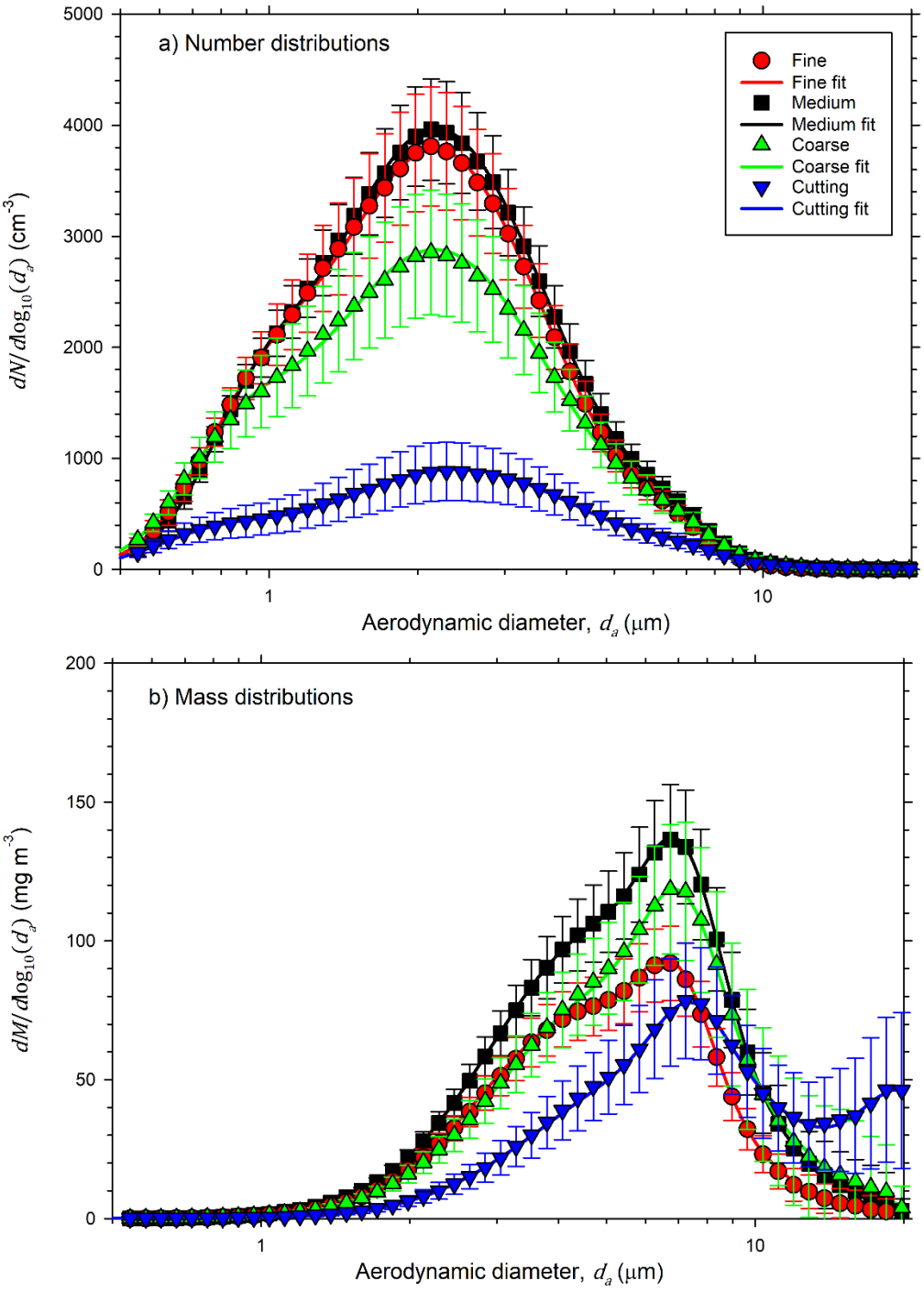

Figure 5. Number-based (a) and mass-based (b) particle size distributions of dust generated during the grinding or cutting of engineered stone. Error bars represent the standard deviation. Curves are best fit multimodal lognormal distributions.

Discussion

Comparison of Particle Size Distributions

In this study, the operation of the cutting blade and all grinding cup wheels generated mass-based size distributions with their most prominent mode located at an aerodynamic diameter of about 4.7 – 6.8 µm (3.8 – 6.4 µm in volume diameter) with the mode increasing with increasing grit coarseness for the grinding cup wheels and being highest for the cutting blade. In the case of the cutting blade, there was a second-most prominent mode at an aerodynamic diameter of 20 µm (19 µm in volume diameter). Two recent related studies have measured the size distributions of dust emissions from engineered stone products with a resin matrix in a controlled environment. Carrieri et al. [2020] investigated stone cutting and Hall et al. [2022] investigated stone cutting and polishing.

Carrieri et al. [2020] measured particle size distributions during engineered stone cutting using an optical particle counter (OPC). The mass-based size distributions had a mode between 3 and 5 µm and a second mode between 10 and 20 µm. However, there are two reasons to believe the size distributions reported are underestimated and, thus, would be in better agreement with the present study if corrected. Firstly, this OPC was factory-calibrated with polystyrene latex spheres and, without proper calibration, undersizes spherical particles having lower refractive indices [Sang-Nourpour and Olfert, 2019]. If we assume that engineered stone dust has a refractive index equal to that of quartz, which is lower than that of polystyrene latex [Hinds, 1999] (and ignore the effects of nonspherical particles), the optical diameter will be smaller than the volume diameter of the particle. Secondly, it appears that in Carrieri et al. [2020] optical particle diameters were erroneously converted to volume diameters using the incorrect assumption that the optical diameter reported by the OPC was instead an aerodynamic diameter (i.e., "the OPC's aerodynamic diameter was converted to the corresponding physical diameter using a shape factor of 1.35 for quartz" (p. 5)). The volume diameter can be related to the aerodynamic diameter using Equation 4 in Appendix I. If we assume Carrieri et al. [2020] assigned a base material density of 2100 kg m^{-3}, as was measured in the present study, this error results in a 20% underreporting in volume diameter. The combined systematic undersizing of particles resulting from these effects may explain why the modes reported by Carrieri et al. [2020] for stone cutting were smaller than those found in the present study.

Hall et al. [2022] measured particle size distributions using an electrical mobility particle sizer for particles 10 to 190 nm in diameter and an OPC for particles 0.25 to 35 µm in diameter during engineered stone cutting and polishing. For comparison with the present study, we will only examine their OPC data. The mass-based size distributions they measured during cutting had modes at 6 and 9 µm and during polishing had a mode of 2.5 µm. While we were unable to find calibration data for this make and model of OPC, it is reasonable to assume that, like described above, optical diameters of particles below a certain size will be smaller than corresponding

volume diameters when the particles' index of refraction is less than that of the particles used for factory calibration [Sorensen et al., 2011].

After the above considerations, we see qualitative agreement between the most prominent mode of the mass-based size distribution during the cutting of engineered stone in the present study (6.4 µm in volume diameter) with those reported by Carrieri et al. [2020] and Hall et al. [2022], as well as for the second-most prominent mode (19 µm in volume diameter) with that report by Carrieri et al. [2020]. The most prominent mode of the mass-based size distribution reported by Hall et al. [2022] for the polishing of engineered stone was smaller than any observed during grinding in the present study. With polishing paper having a finer grit than any of grinding cup wheels investigated in this study, this follows the trend of particle size distributions shifting to larger sizes for increasing coarseness of grit (2.5 µm optical diameter for polishing [Hall et al., 2022]; 3.8 µm volume diameter for fine grit grinding cup wheel; 4.3 µm volume diameter for medium grit grinding cup wheel; 4.7 µm volume diameter for coarse grit grinding cup wheel). This, together with our previous results for the grinding of natural and engineered stone products [NIOSH, 2023], suggests that the mechanical process of the fabrication task predominantly determines the shape of the dust size distribution. We see that different fabrication tasks (e.g., cutting, grinding, and polishing) can lead to airborne dust with varying size distribution shapes. When investigating the removal mechanisms in the sawing and grinding [Xu et al., 2003] and polishing [Saidi et al., 2015] of granite, it was observed that brittle fracture was the dominant mechanism for coarse grit sizes while ductile flow was the dominant mechanism for finer grit sizes. Perhaps a more thorough investigation of the relationships between processing parameters (e.g., abrasive grit size, feed rates, cutting forces, tool rotational speeds, etc.) and engineered stone product properties (e.g., hardness, silica content, etc.) and the resulting dust emissions would be possible. This could be achieved by combining the computer numerical control (CNC) machining approach of Saidi et al. [2015], which can control and/or measure processing parameters, with the laboratory testing system used in this study to characterize emissions.

Comparison of Crystalline Silica Content

There was no statistically significant difference in the crystalline silica content of the respirable dust generated from engineered stone by each of the angle grinder discs (grinding cup wheels with fine, medium, and coarse grit and a cutting blade). Hall et al. [2022] reported that the crystalline silica content in respirable dust generated by cutting was higher than that from polishing for all engineered and natural stone products investigated. This might be partially attributable to 1) the effect of particle size on the quantification of crystalline silica by XRD and 2) different fabrication tasks generating airborne dusts with varying size distributions. Rishi et al. [2024] found that XRD response to size-classified quartz and cristobalite standard reference materials decreased with decreasing particle aerodynamic diameter in the investigated range of approximately 50 nm to 10 µm. The mass-based particle size distributions generated in the present study by each angle grinder disc differed little, especially if only considering the distribution of respirable particle mass (see

Figure 7, estimated using the procedure outlined in Appendix I). With very similar size distributions, the particle size-dependency of XRD would affect all samples equally. In contrast, the mass-based size distributions measured by Hall et al. [2022] during polishing had their major peak at 0.1 µm with a secondary peak at 2.5 µm, while the major peaks during cutting were at 6 – 9 µm. The shift in particle size distributions toward smaller particles during polishing versus cutting could have resulted in a lower XRD response and, correspondingly, a lower measured crystalline silica content.

Comparison of Normalized Generation Rates

Using a normalized generation rate as a metric for characterizing the emissions from subtractive processes (e.g., grinding, sanding, and cutting) enables comparison of emissions from different studies on different tasks and provides valuable input parameters for modeling workplace exposure. Nominal values of concentrations will be dependent on the dilution occurring in the testing system used to generate the data. In contrast, the generation rate obtained by following the European Standard EN 1093-3 [CEN, 2006] is independent of system dilution rates and allows for comparisons between studies. In determining a normalized generation rate, the nominal generation rate, represented in mass per unit of time, is normalized by a measure of work task productivity. In this study, as in our previous studies on the sawing [Kang et al., 2019] and sanding [Kang et al., 2020] of solid surface composite material and the grinding of engineered and natural stone products [NIOSH, 2023], the measure of productivity was the material removal rate (see Figure 4 for the material removal rates measured in this study). Because the nominal generation rate and material removal rate share the same denominator, we can define the normalized generation rate in Equation 1 as the mass of emissions generated per unit of volume removed from the workpiece. The volume removed from workpieces by grinding or cutting might be estimated from geometric measurements and/or countertop design features (e.g., dimensions of slabs, dimensions of cutouts, radii of corners, edge profiles, etc.). With the normalized generation rate, the RCS mass generated by a worker during the full-shift may be derived, which may then be readily incorporated into a model to estimate the worker's RCS exposure after consideration of aerosol dispersion, background concentration, and other modeling factors. Furthermore, by comparing the normalized generation rate with and without the use of different exposure control measures, the effectiveness of the control measures can be evaluated. Such an approach will allow prompt identification and optimization of feasible control measures in a standard laboratory setting prior to more expensive field validations, as was done by a study from NIOSH [2014] on controlling RCS exposures from cutting fiber-cement.

For identical amounts of materials removed from grinding and cutting activities within similar time frames, a worker's time-weighted-average RCS exposure is likely to be commensurate with the normalized generation rate of RCS for a given identical stone product in the same workplace setting. Among the four angle grinder discs that were studied, the normalized generation rate of RCS was lowest for the cutting blade and increased with finer grit sizes for the grinding cup wheels.

Because we only considered swarf (i.e., debris made by grinding and cutting) when determining the volume removed from the workpiece, this is a conservative estimate of the normalized generation rate of RCS during cutting. In practice, there would be a significant volume of material removed on the waste side of the cut. These results indicate that prioritizing cutting over grinding, when feasible, may minimize RCS exposures. Furthermore, when using grinding cup wheels, the prioritization of coarser grits, whenever suitable, may minimize RCS exposures. Thus, rough grinding might best be performed with as coarse of grit as possible; whereas finer grits might best be reserved for whenever more precise operation of the grinder or smoother surfaces are required.

Conclusions and Recommendations

Controlling exposures to occupational hazards is the fundamental method of protecting workers. Traditionally, a hierarchy of controls has been used as a means of determining how to implement feasible and effective controls. One representation of the hierarchy of controls can be summarized as follows:

- Elimination
- Substitution
- Engineering Controls (e.g., ventilation)
- Administrative Controls (e.g., reduced work schedules)
- Personal Protective Equipment (PPE, e.g., respirators)

The idea behind this hierarchy is that the control methods at the top of the list are potentially more effective, protective, and economical (in the long run) than those at the bottom. Following the hierarchy normally leads to the implementation of inherently safer systems, ones where the risk of illness or injury has been substantially reduced.

Normalized RCS generation rates indicate that when removing the same volume of engineered stone by grinding or cutting activities, workers are likely to be exposed to lower quantities of RCS when cutting with a cutting blade, followed by grinding with a coarse grit grinding cup wheel, then grinding with a medium grit grinding cup wheel, and, finally, grinding with a fine grit grinding cup wheel. This suggests that an appropriate administrative control could be to train workers to prioritize cutting over grinding, when feasible, and when grinding prioritize grinding cup wheels with coarser grits whenever suitable for the surface finish required. This approach likely aligns with the workflow already used by most stone countertop fabricators, as it also maximizes the workpiece removal rate–a measure of process productivity. Administrative controls work best when combined with the more effective methods of elimination, substitution, and engineering controls.

References

81 Fed. Reg. 16285 [2016]. Occupational Safety and Health Administration: occupational exposure to respirable crystalline silica, final rule.

https://www.federalregister.gov/documents/2016/03/25/2016-04800/occupational-exposure-to-respirable-crystalline-silica

Blatt H, Tracy R [1997]. Petrology: igneous, sedimentary and metamorphic (2nd ed.). New York, NY: W.H. Freeman and Company. p. 66.

Branch MA, Coleman TF, Li Y [1999]. A Subspace, Interior, and Conjugate Gradient Method for Large-Scale Bound-Constrained Minimization Problems. SIAM J Sci Comput*,* 21(1): 1-23.

Brockmann JE [2011]. Aerosol Transport in Sampling Lines and Inlets. *In:* Kulkarni P, Baron PA, Willeke K Eds. Aerosol measurement : principles, techniques, and applications). Hoboken, NJ: John Wiley & Sons, Inc. p. 69.

Bureau of Mines [1992]. Crystalline Silica Primer. Washington, DC: U.S. Department of the Interior, Bureau of Mines, Branch of Industrial Minerals. Special Publication

Carrieri M, Guzzardo C, Farcas D, Cena LG [2020]. Characterization of Silica Exposure during Manufacturing of Artificial Stone Countertops. Int J Environ Res Public Health*,* 17(12): 4489.

CEN [2006]. EN 1093-3, Safety of machinery - Evaluation of the emission of airborne hazardous substances - Part 3: Test bench method for the measurement of the emission rate of a given pollutant. Brussels, Belgium: European Committee for Standardization.

Cheng Y-S, Yeh H-C, Allen MD [1988]. Dynamic Shape Factor of a Plate-Like Particle. Aerosol Sci Technol*,* 8(2): 109-123.

Davies CN [1979]. Particle-fluid interaction. J Aerosol Sci*,* 10(5): 477-513.

Fazio JC, Gandhi SA, Flattery J, Heinzerling A, Kamangar N, Afif N, Cummings KJ, et al. [2023]. Silicosis Among Immigrant Engineered Stone (Quartz) Countertop Fabrication Workers in California. JAMA Internal Medicine*,* 183(9): 991-998.

Friedman G, Harrison R, Bojes H, Worthington K, Filios M [2015]. Notes from the field: silicosis in a countertop fabricator—Texas, 2014. Morbidity and Mortality Weekly Report*,* 64: 129-130.

Glass DC, Dimitriadis C, Hansen J, Hoy RF, Hore-Lacy F, Sim MR [2022]. Silica Exposure Estimates in Artificial Stone Benchtop Fabrication and Adverse Respiratory Outcomes. Ann Work Expo Health*,* 66(1): 5-13.

Hall S, Stacey P, Pengelly I, Stagg S, Saunders J, Hambling S [2022]. Characterizing and Comparing Emissions of Dust, Respirable Crystalline Silica, and Volatile Organic Compounds from Natural and Artificial Stones. Ann Work Expo Health*,* 66(2): 139-149.

Hatch T, Choate SP [1929]. Statistical description of the size properties of non uniform particulate substances. J Franklin Inst*,* 207(3): 369-387.

Hinds WC [1999]. Aerosol technology: properties, behavior, and measurement of airborne particles. New York, NY: John Wiley & Sons, Inc.

International Organization for Standardization [2008]. Uncertainty of measurement-Part 3: Guide to the expression of uncertainty in measurement (GUM: 1995). Switzerland: ISO.

Kang S, Liang H, Qian Y, Qi C [2019]. The Composition of Emissions from Sawing Corian®, a Solid Surface Composite Material. Ann Work Expo Health*,* 63(4): 480-483.

Kang S, Liang H, Qian Y, Qi C [2020]. The Composition of Emissions from Sanding Corian® with Different Sandpapers. Aerosol and Air Quality Research*,* 20.

Kramer MR, Blanc PD, Fireman E, Amital A, Guber A, Rhahman NA, Shitrit D [2012]. Artificial Stone Silicosis: Disease Resurgence Among Artificial Stone Workers. Chest*,* 142(2): 419-424.

Lofgren DJ [2008]. Results of Inspections in Health Hazard Industries in a Region of the State of Washington. J Occup Environ Hyg*,* 5(6): 367-379.

Marshall IA, Mitchell JP, Griffiths WD [1991]. The behaviour of regular-shaped non-spherical particles in a TSI aerodynamic particle sizer. J Aerosol Sci*,* 22(1): 73-89.

NIOSH [1986]. Occupational respiratory diseases. Cincinnati, OH: U.S. Department of Health and Human Services, Public Health Service, Centers for Disease Control and Prevention, National Institute for Occupational Safety and Health, DHHS (NIOSH) Publication No. 86-102.

NIOSH [1998]. Particles not otherwise regulated, respirable. NIOSH Manual of Analytical Methods (NMAM®), 4th ed., 2nd Supplement, Schlecht PC, O'Connor PF Eds. Cincinnati, OH: U.S. Department of Health and Human Services, Public Health Service, Centers for Disease Control and Prevention, National Institute for Occupational Safety and Health, National Institute for Occupational Safety and Health, DHHS (NIOSH) Publication No. 98-119.

NIOSH [2002]. NIOSH Hazard Review: Health Effects of Occupational Exposure to Respirable Crystalline Silica. Cincinnati, OH: U.S. Department of Health and Human Services, Public Health Service, Centers for Disease Control and Prevention, National Institute for Occupational Safety and Health, DHHS (NIOSH) Publication No. 98-119.

NIOSH [2003]. SILICA, CRYSTALLINE, by XRD (filter redeposition). NIOSH Manual of Analytical Methods (NMAM®), 4th ed., 3rd Supplement, Schlecht PC, O'Connor PF Eds. Cincinnati, OH: U.S. Department of Health and Human Services, Public Health

Service,, Centers for Disease Control and Prevention, National Institute for Occupational Safety and Health, DHHS (NIOSH) Publication No. 2003-154.

NIOSH [2014]. Evaluation of the dust generation and engineering control for cutting fiber-cement siding. By Qi C, Echt A, Gressel M, Feng HA. Cincinnati, OH: U.S. Department of Health and Human Services, Centers for Disease Control and Prevention, National Institute for Occupational Safety and Health, EPHB Report No. 358-16a. https://www.cdc.gov/niosh/surveyreports/pdfs/358-16a.pdf

NIOSH [2016a]. Evaluation of Crystalline Silica Exposure during Fabrication of Natural and Engineered Stone Countertops. By Zwack LM, Victory KR, Brueck SE, Qi C. Cincinnati, OH: U.S. Department of Health and Human Services, Centers for Disease Control and Prevention, National Institute for Occupational Safety and Health, HHE Report No. 2014-0215-3250. https://www.cdc.gov/niosh/hhe/reports/pdfs/2014-0215-3250.pdf

NIOSH [2016b]. Engineering Control of Silica Dust from Stone Countertop Fabrication and Installation, In-depth field survey report for the Houston, TX field survey. By Qi C, Echt A. Cincinnati, OH: U.S. Department of Health and Human Services, Centers for Disease Control and Prevention, National Institute for Occupational Safety and Health, EPHB Report NO. 375-11a. https://www.cdc.gov/niosh/surveyreports/pdfs/375-11a.pdf

NIOSH [2016c]. Engineering Control of Silica Dust from Stone Countertop Fabrication and Installation, In-depth field survey report for the Mendota Heights, MN field survey. By Qi C, Lo L. Cincinnati, OH: Department of Health and Human Services, Centers for Disease Control and Prevention, National Institute for Occupational Safety and Health, EPHB Report No. 375-12a. https://www.cdc.gov/niosh/surveyreports/pdfs/375-12a.pdf

NIOSH [2021]. Engineering Control of Silica Dust from Stone Countertop Fabrication and Installation – Evaluation of Wetting Methods for Grinding. By Qi C, Echt A. Cincinnati, OH: U.S. Department of Health and Human Services, Centers for Disease Control and Prevention, National Institute for Occupational Safety and Health, EPHB Report NO. 2021-DFSE-710. https://www.cdc.gov/niosh/surveyreports/pdfs/2021-DFSE-710.pdf

NIOSH [2023]. Characterization of Airborne Dust Generated from the Grinding of Natural and Engineered Stone Products. By Thompson D, Qi C. Cincinnati, OH: U.S. Department of Health and Human Services, Centers for Disease Control and Prevention, National Institute for Occupational Safety and Health, EPHB Report No. 2023-DFSE-1489.

NIOSH, OSHA [2015]. Worker exposure to silica during countertop manufacturing, finishing and installation. National Institute for Occupational Safety and Health, Occupational Safety and Health Administration, DHHS (NIOSH) Publication No. 2015–106, OSHA HA–3768–2015. https://www.osha.gov/sites/default/files/publications/OSHA3768.pdf.

Pérez-Alonso A, Córdoba-Doña JA, Millares-Lorenzo JL, Figueroa-Murillo E, García-Vadillo C, Romero-Morillo J [2014]. Outbreak of silicosis in Spanish quartz conglomerate workers. Int J Occup Environ Health, 20(1): 26-32.

Phillips ML, Johnson AC [2012]. Prevalence of Dry Methods in Granite Countertop Fabrication in Oklahoma. J Occup Environ Hyg, 9(7): 437-442.

Phillips ML, Johnson DL, Johnson AC [2013]. Determinants of Respirable Silica Exposure in Stone Countertop Fabrication: A Preliminary Study. J Occup Environ Hyg, 10(7): 368-373.

Qi C, Echt A, Gressel MG [2016]. On the Characterization of the Generation Rate and Size-Dependent Crystalline Silica Content of the Dust from Cutting Fiber Cement Siding. Ann Occup Hyg, 60(2): 220-30.

Qi C, Thompson D, Amy Feng H [2022]. Caution on Using Tetrahydrofuran for Processing Crystalline Silica Samples From Engineered Stone for XRD Analysis. Ann Work Expo Health, 66(9): 1210-1214.

Rishi K, Ku BK, Qi C, Thompson D, Wang C, Dozier A, Vogiazi V, et al. [2024]. Release of Crystalline Silica Nanoparticles during Engineered Stone Fabrication. ACS Omega, 9(51): 50308-50317.

Rose C, Heinzerling A, Patel K, Sack C, Wolff J, Zell-Baran L, Weissman D, et al. [2019]. Severe silicosis in engineered stone fabrication workers—California, Colorado, Texas, and Washington, 2017–2019. Morbidity and Mortality Weekly Report, 68(38): 813.

Saidi MN, Songmene V, Kouam J, Bahloul A [2015]. Experimental investigation on fine particle emission during granite polishing process. Int J Adv Manuf Technol, 81(9): 2109-2121.

Sang-Nourpour N, Olfert JS [2019]. Calibration of optical particle counters with an aerodynamic aerosol classifier. J Aerosol Sci, 138: 105452.

Seinfeld JH, Pandis SN [2016]. Atmospheric chemistry and physics: from air pollution to climate change. John Wiley & Sons.

Sorensen CM, Gebhart J, O'Hern TJ, Rader DJ [2011]. Optical Measurement Techniques: Fundamentals and Applications. *In:* Aerosol measurement : principles t, and applications Ed. Hoboken, NJ). John Wiley & Sons, Inc. p. 269.

Thompson D, Qi C [2023]. Characterization of the Emissions and Crystalline Silica Content of Airborne Dust Generated from Grinding Natural and Engineered Stones. Ann Work Expo Health, 67(2): 266-280.

TSI Incorporated [2013]. Aerosol Instrument Manager® Software for Aerodynamic Particle Sizer® (APS™) Spectrometers, P/N 1930064, REVISION H.

Vincent JH [2007]. Aerosol sampling : science, standards, instrumentation and applications. Chichester, England: John Wiley & Sons Ltd.

Virtanen P, Gommers R, Oliphant TE, Haberland M, Reddy T, Cournapeau D, Burovski E, et al. [2020]. SciPy 1.0: fundamental algorithms for scientific computing in Python. Nat Methods*,* 17(3): 261-272.

Wang H-C, John W [1987]. Particle Density Correction for the Aerodynamic Particle Sizer. Aerosol Sci Technol*,* 6(2): 191-198.

Xu XP, Huang H, Li Y [2003]. Material Removal Mechanisms in Diamond Grinding of Granite, Part 1: The Morphological Changes of Granite from Sawing to Grinding. Key engineering materials*,* 250: 215-221.

Appendices

Appendix I. Treatment of APS Data

The particle shape and density correction for the APS outlined by Marshall et al. [1991] is identical to the density correction algorithm that is implemented into AIM [Wang and John, 1987] if the particle density, ρ_p, is replaced by the particle density divided by the dynamic shape factor, ρ_p/χ. In this study, particle density and dynamic shape factor were assumed to be particle size-independent and particle density was assumed to be equal to the bulk material density of the stone samples.

Particle dynamic shape factor was unknown and found in the following manner. The mass in APS channel i at time t, $m_{i,t}$, was found using Equation 3 where $n_{i,t}$ is the particle count in channel i at time t and d_{v_i} is the particle volume diameter at the midpoint of channel i.

$$m_{i,t} = \frac{\pi}{6}\rho_p n_{i,t} d_{v_i}^3 \qquad \textbf{Equation 3}$$

Particle volume diameter was related to the particle aerodynamic diameter, d_a, by Equation 4 where ρ_0 is a standard density of 1000 kg m^{-3} [Hinds, 1999].

$$d_v = d_a \sqrt{\chi \frac{\rho_0}{\rho_p}} \qquad \textbf{Equation 4}$$

The respirable mass sampled by the APS, $m_{APS,respir}$, was then found by Equation 5 where R_i is the ACGIH criterion for the respirable fraction [Vincent, 2007] calculated at the midpoint of channel i.

$$m_{APS,respir} = \sum_t \sum_i R_i m_{i,t} \qquad \textbf{Equation 5}$$

The sum of the squared residuals, S, was then determined using Equation 6 where $\bar{m}_{sampl_j}$ is the average respirable mass collected by the respirable samplers in experiment run j, Q_{sampl} is the flowrate of the respirable sampler (9.0 l min^{-1}), and Q_{APS} is the aerosol sample flowrate in the APS (1.0 l min^{-1}).

$$S = \sum_{j=1}^{3} \left(\bar{m}_{sampl_j} - \frac{Q_{sampl}}{Q_{APS}} m_{APS,respir_j} \right)^2 \qquad \textbf{Equation 6}$$

The estimated dynamic shape factor was then identified by minimizing the sum of the squared residuals as demonstrated in Figure 6. The best fit dynamic shape factors are listed in Table 4 and ranged from 1.4 to 1.9. For the grinding cup wheels the dynamic shape factor increased with increasing coarseness of grit. The cutting blade produced particles with the highest dynamic shape factor. These values were comparable to those found by Davies [1979] for quartz (1.36) and sand (1.57) and by Cheng et al. [1988] for talc (1.88).

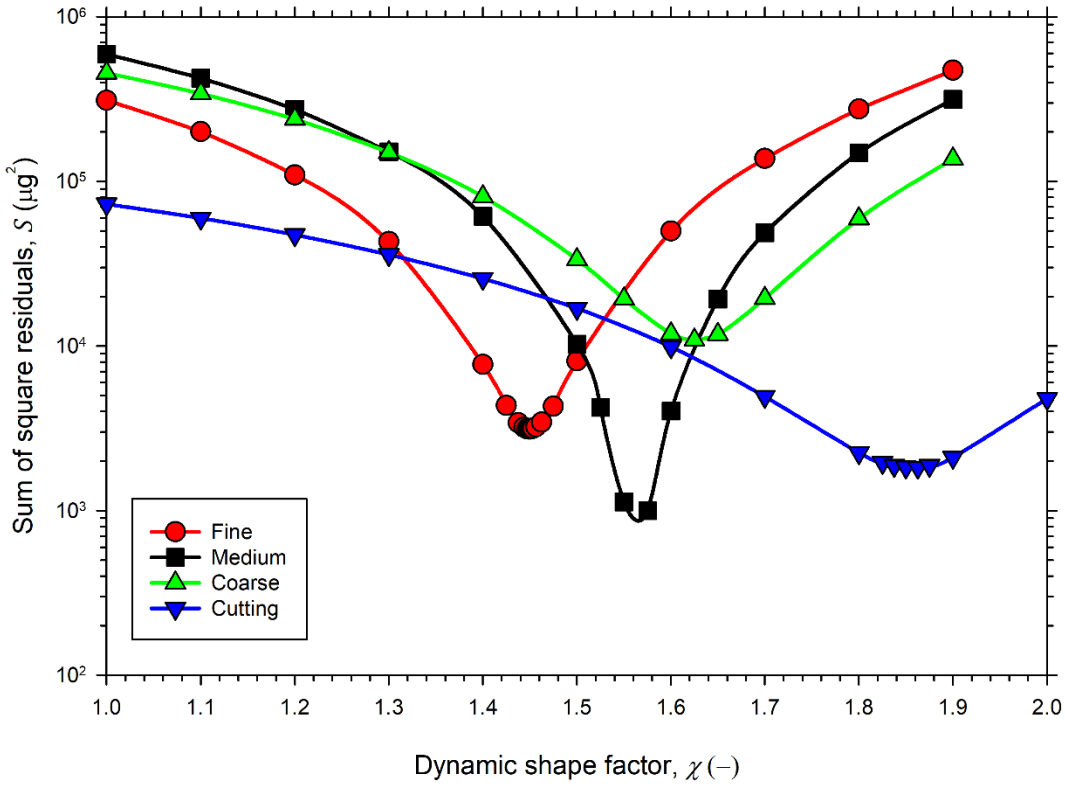

Figure 6. Sum of squared residuals from APS-derived respirable mass as a function of particle dynamic shape factor for grinding or cutting engineered stone. Plotted curves are simple spline curves generated by SigmaPlot (v14.5, Inpixon, USA).

After correcting for particle shape and density, the particle number distribution measurements, $dN/d\log_{10}(d_a)$, were averaged over the periods of active grinding from the three experimental runs. Particle size distributions expressed as a function of the common logarithm of the particle diameter were related to size distributions as a function of the natural logarithm of particle diameter by $dN/d\log_{10}(d_a) = \ln(10)\, dN/d\ln(d_a)$ [Seinfeld and Pandis, 2016]. Number-based, multimodal lognormal size distribution functions, as defined in Equation 7, were then fit to the APS-measured number-based particle size distributions and standard deviations using the Trust Region Reflective minimization algorithm [Branch et al., 1999] implemented in the Python package SciPy [Virtanen et al., 2020]. Here, N_i is the number concentration of mode i, CMD_i is the count median aerodynamic diameter of mode i, and σ_{g_i} is the geometric standard deviation of mode i.

$$f_N(\ln d_a) = \sum_{i=1}^{n} \frac{N_i}{\sqrt{2\pi}\ln\sigma_{g_i}} \exp\left[-\frac{(\ln d_a - \ln CMD_i)^2}{2\left(\ln\sigma_{g_i}\right)^2}\right] \qquad \textbf{Equation 7}$$

A mass-based, multimodal lognormal size distribution, as shown in Equation 8, was then derived from the parameters of the best fit number-based lognormal size distribution. Here, M_i is the mass concentration of mode i and MMD_i is the mass median aerodynamic diameter of mode i.

$$f_M(\ln d_a) = \sum_{i=1}^{n} \frac{M_i}{\sqrt{2\pi}\ln\sigma_{g_i}} \exp\left[-\frac{(\ln d_a - \ln MMD_i)^2}{2\left(\ln\sigma_{g_i}\right)^2}\right] \quad \textbf{Equation 8}$$

Equation 9 was used to calculate M_i where $d_{\bar{m}_i}$ is the particle diameter of average mass of mode i.

$$M_i = \frac{\pi}{6}\rho_p d_{\bar{m}_i}^3 N_i \quad \textbf{Equation 9}$$

The diameters of average mass and mass median diameters were found using the Hatch-Choate equations [Hatch and Choate, 1929; Hinds, 1999] in Equation 10 and 11, respectively, where CMD_{v_i} is the count median volume diameter of mode i. The count median aerodynamic diameter and count median volume diameter were related using Equation 4.

$$d_{\bar{m}_i} = CMD_{v_i} \exp\left[\frac{3}{2}\left(\ln\sigma_{g_i}\right)^2\right] \quad \textbf{Equation 10}$$

$$MMD_i = CMD_i \exp\left[3\left(\ln\sigma_{g_i}\right)^2\right] \quad \textbf{Equation 11}$$

Parameters for the best fit number-based distributions are summarized in Table 4. For convenience, the total number concentration, $N_T = \sum_{i=1}^{n} N_i$, was factored out of the results to allow for easier comparisons of the weight of each mode, $w_{N_i} = N_i/N_T$, when reporting results. The derived, mass-based, multimodal lognormal distribution parameters are summarized in Table 5. Again, the total mass concentration, $M_T = \sum_{i=1}^{n} M_i$, was factored out of the results to allow for easier comparisons of the weight of each mode, $w_{M_i} = M_i/M_T$, when reporting results.

Table 4. Best fit dynamic shape factor and number-based, multimodal lognormal distribution parameters (and resulting coefficient of determination, R^2) for particle size distributions measured by APS

Disc	χ (-)	N_T (cm^{-3})	w_{N_1} (-)	CMD_1 (μm)	σ_{g_1} (-)	w_{N_2} (-)	CMD_2 (μm)	σ_{g_2} (-)	w_{N_3} (-)	CMD_3 (μm)	σ_{g_3} (-)	w_{N_4} (-)	CMD_4 (μm)	σ_{g_4} (-)	R^2 (-)
Fine	1.4	2400	0.115	0.924	1.32	0.870	2.18	1.66	0.0153	6.42	1.18	–	–	–	1.0
Medium	1.6	2510	0.0794	0.926	1.27	0.904	2.18	1.69	0.0168	6.57	1.19	–	–	–	1.0
Coarse	1.6	1970	0.108	0.855	1.30	0.873	2.17	1.73	0.0183	6.54	1.19	–	–	–	1.0
Cutting	1.9	670	0.118	0.773	1.34	0.862	2.39	1.80	0.0178	6.90	1.18	0.00188	17.8	1.23	1.0

Table 5. Derived, mass-based, multimodal lognormal distribution parameters (and resulting coefficient of determination, R^2) for particle size distributions measured by APS

Disc	M_T (mg m^{-3})	w_{M_1} (-)	MMD_1 (μm)	w_{M_2} (-)	MMD_2 (μm)	w_{M_3} (-)	MMD_3 (μm)	w_{M_4} (-)	MMD_4 (μm)	R^2 (-)
Fine	47.9	0.00385	1.16	0.859	4.67	0.137	6.99	–	–	1.0
Medium	69.5	0.00215	1.10	0.854	4.98	0.144	7.20	–	–	1.0
Coarse	58.3	0.00228	1.05	0.853	5.37	0.145	7.17	–	–	1.0
Cutting	47.7	0.00106	0.995	0.740	6.77	0.0879	7.47	0.171	20.3	1.0

Appendix II. Additional Tables and Figures

Table 6. p-values from Welch's ANOVA test to determine whether means of the RCS content, respirable dust normalized generation rates, RCS normalized generation rates, and material removal rates were equal for all angle grinder discs

	Crystalline silica content of respirable dust	Respirable dust normalized generation rate	RCS normalized generation rate	Material removal rate
Sample size	24	24	24	3
p-values	0.78	6.9E-18	1.0E-16	0.0054

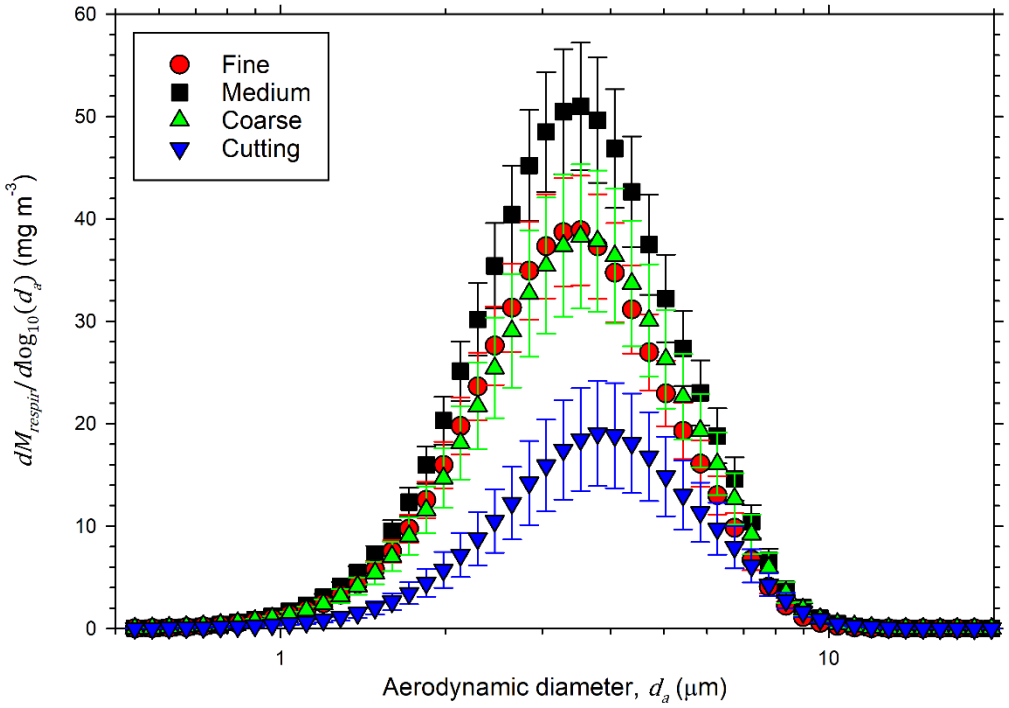

Figure 7. Mass-based particle size distributions of respirable dust mass during the grinding or cutting of engineered stone

Appendix III. Tabulated Data from Figures

Table 7. Crystalline silica content of respirable dust

Disc	Cristobalite content (wt%)		Quartz content (wt%)		Crystalline silica content (wt%)	
	Average	Combined standard uncertainty	Average	Combined standard uncertainty	Average	Combined standard uncertainty
Fine	44	12	20.2	5.5	64	15
Medium	46	12	20.5	5.3	66	15
Coarse	47	15	21.3	6.5	68	19
Cutting	44	18	18.5	7.9	63	23

Table 8. Normalized generation rates

Disc	RCS (mg cm^{-3})		Respirable dust (mg cm^{-3})	
	Average	Combined standard uncertainty	Average	Combined standard uncertainty
Fine	24.2	5.9	38.5	7.2
Medium	20.0	3.6	30.5	5.8
Coarse	14.2	3.1	21.0	4.9
Cutting	9.4	3.0	15.2	4.8

Table 9. Material removal rates

Disc	Average (cm^3 min^{-1})	Standard deviation (cm^3 min^{-1})
Fine	5.00	0.55
Medium	7.62	0.31
Coarse	9.21	0.72
Cutting	6.04	0.70

Table 10. Particle number-based size distributions from APS

Midpoint aerodynamic diameter, d_a (µm)	$dN/d\log_{10}(d_a)$ (cm^{-3})							
	Fine		Medium		Coarse		Cutting	
	Avg	StDev	Avg	StDev	Avg	StDev	Avg	StDev
0.542	216	70	174	53	270	53	151	41
0.583	346	98	286	77	422	77	212	58
0.626	510	120	442	97	600	110	268	78
0.673	730	120	650	110	810	140	321	95
0.723	970	120	900	110	1000	180	360	110
0.777	1240	130	1200	110	1190	230	390	120
0.835	1480	150	1440	120	1350	260	420	130
0.898	1720	190	1700	150	1500	300	440	140
0.965	1910	230	1910	170	1600	330	450	140
1.037	2110	280	2130	210	1730	350	480	150
1.114	2290	310	2320	240	1840	380	510	160
1.197	2490	350	2530	260	1970	400	550	170
1.286	2710	390	2760	290	2120	430	590	190
1.382	2890	410	2960	320	2240	460	630	200
1.486	3080	440	3180	350	2370	480	680	220
1.596	3270	470	3380	370	2500	500	720	230
1.715	3440	490	3570	400	2610	520	770	240
1.843	3610	510	3750	430	2720	540	810	250
1.981	3750	530	3900	450	2820	560	850	260
2.129	3810	540	3960	460	2860	560	880	260
2.288	3760	530	3930	460	2830	550	880	260
2.458	3660	510	3840	450	2760	530	880	260
2.642	3480	480	3680	440	2640	500	860	250
2.839	3290	450	3490	420	2520	480	850	240
3.051	3020	410	3210	390	2350	440	820	230
3.278	2730	370	2910	350	2150	400	780	220
3.523	2420	330	2600	320	1950	360	730	200
3.786	2090	290	2270	280	1730	320	670	180
4.068	1780	250	1970	240	1530	280	610	170
4.371	1490	210	1670	210	1320	240	550	150
4.698	1230	170	1400	180	1120	200	480	130
5.048	1020	140	1170	160	960	180	420	110
5.425	860	120	990	130	820	150	366	95
5.829	730	100	850	120	720	130	326	83
6.264	620	89	730	100	630	120	293	76
6.732	503	74	612	89	530	100	257	67
7.234	380	58	483	74	425	90	219	58
7.774	261	42	350	58	313	76	174	45
8.354	166	30	236	44	215	62	129	35
8.977	101	20	149	32	139	48	91	26
9.647	60	14	91	24	87	38	62	19
10.37	35	10	55	18	55	30	43	15
11.14	20.5	7.7	34	14	35	23	30	12
11.97	11.8	5.6	20	10	22	18	22	10
12.86	7.6	4.8	12.7	7.5	14	14	16.8	7.6
13.82	4.6	3.3	8.1	6.3	9	12	13.7	6.7
14.86	2.8	2.7	5.0	4.9	6.6	9.8	11.4	5.9
15.96	1.9	2.3	3.3	3.8	4.5	7.3	9.6	5.4
17.15	1.1	1.7	2.2	3.0	3.1	5.0	8.7	4.9
18.43	0.7	1.2	1.4	2.1	2.1	3.7	7.8	4.4
19.81	–	–	0.46	0.80	0.7	1.4	6.3	3.8

Table 11. Particle mass-based size distributions from APS

Midpoint aerodynamic diameter, d_a (µm)	$dM/d\log_{10}(d_a)$ (mg m^{-3})							
	Fine		Medium		Coarse		Cutting	
	Avg	StDev	Avg	StDev	Avg	StDev	Avg	StDev
0.542	0.0205	0.0067	0.0203	0.0062	0.0315	0.0062	0.0228	0.0062
0.583	0.041	0.012	0.041	0.011	0.061	0.011	0.040	0.011
0.626	0.075	0.017	0.079	0.017	0.108	0.019	0.062	0.018
0.673	0.134	0.022	0.146	0.025	0.182	0.032	0.093	0.027
0.723	0.220	0.027	0.249	0.031	0.279	0.050	0.129	0.040
0.777	0.347	0.036	0.403	0.039	0.410	0.078	0.173	0.054
0.835	0.517	0.053	0.615	0.052	0.58	0.11	0.229	0.073
0.898	0.746	0.082	0.900	0.077	0.79	0.16	0.30	0.10
0.965	1.03	0.13	1.25	0.11	1.05	0.21	0.39	0.12
1.037	1.41	0.18	1.74	0.17	1.41	0.29	0.51	0.16
1.114	1.90	0.26	2.34	0.24	1.86	0.38	0.66	0.21
1.197	2.56	0.36	3.18	0.33	2.47	0.51	0.89	0.28
1.286	3.45	0.49	4.30	0.46	3.29	0.68	1.18	0.38
1.382	4.56	0.65	5.73	0.62	4.32	0.89	1.58	0.50
1.486	6.05	0.86	7.64	0.83	5.7	1.2	2.12	0.67
1.596	8.0	1.1	10.1	1.1	7.4	1.5	2.78	0.87
1.715	10.4	1.5	13.2	1.5	9.6	1.9	3.7	1.1
1.843	13.5	1.9	17.2	2.0	12.5	2.5	4.8	1.5
1.981	17.4	2.5	22.2	2.5	16.0	3.2	6.3	1.9
2.129	22.0	3.1	28.0	3.2	20.2	4.0	8.0	2.4
2.288	27.0	3.8	34.4	4.0	24.8	4.8	10.0	3.0
2.458	32.5	4.5	41.7	4.9	30.0	5.8	12.4	3.7
2.642	38.4	5.3	49.6	5.9	35.7	6.8	15.0	4.4
2.839	45.1	6.2	58.4	7.0	42.2	8.0	18.4	5.3
3.051	51.4	7.0	66.7	8.1	48.8	9.1	21.9	6.2
3.278	57.5	7.9	75.0	9.1	56	10	25.9	7.2
3.523	63.4	8.7	83	10	62	11	30.1	8.2
3.786	67.8	9.3	90	11	69	13	34.6	9.3
4.068	72	10	97	12	75	14	39	11
4.371	75	10	102	13	81	15	43	12
4.698	76	11	106	14	85	16	48	12
5.048	79	11	111	15	90	16	51	13
5.425	82	12	116	16	96	18	55	14
5.829	87	12	124	17	104	19	61	16
6.264	91	13	132	19	113	21	68	18
6.732	92	13	137	20	119	23	74	19
7.234	86	13	134	20	118	25	78	21
7.774	74	12	120	20	107	26	77	20
8.354	58	10	101	19	92	26	71	19
8.977	43.9	8.5	79	17	73	26	63	18
9.647	32.2	7.4	60	15	57	25	53	16
10.37	23.1	6.7	45	14	45	24	45	16
11.14	17.0	6.4	34	14	35	23	40	15
11.97	12.1	5.8	25	12	28	23	36	16
12.86	9.7	6.1	20	12	22	22	34	15
13.82	7.2	5.3	16	12	18	22	34	17
14.86	5.5	5.3	12	12	16	24	35	18
15.96	4.6	5.7	10	11	13	22	37	21
17.15	3.2	5.0	8	11	11	18	41	24
18.43	2.6	4.6	7	10	10	17	46	26
19.81	–	–	2.6	4.5	3.9	7.8	46	28

Table 12. Sum of squared residuals from APS-derived respirable mass as a function of particle dynamic shape factor

Fine		Medium		Coarse		Cutting	
χ (-)	S (μg^2)	χ (-)	S (μg^2)	χ (-)	S (μg^2)	χ (-)	S (μg^2)
1	311000	1	593000	1	456000	1	72800
1.1	200000	1.1	424000	1.1	342000	1.1	59800
1.2	109000	1.2	275000	1.2	239000	1.2	47500
1.3	43000	1.3	151000	1.3	150000	1.3	35900
1.4	7740	1.4	61500	1.4	80900	1.4	25700
1.425	4360	1.5	10300	1.5	33600	1.5	16900
1.4375	3410	1.525	4240	1.55	19400	1.6	9900
1.44375	3210	1.55	1130	1.6	11900	1.7	4930
1.446875	3140	1.575	999	1.625	10900	1.8	2250
1.4484375	3130	1.6	4030	1.65	11800	1.825	1960
1.44921875	3130	1.65	19300	1.7	19500	1.8375	1880
1.45	3130	1.7	48800	1.8	59500	1.85	1840
1.4515625	3140	1.8	149000	1.9	137000	1.8625	1840
1.453125	3160	1.9	316000			1.875	1880
1.45625	3220					1.9	2110
1.4625	3450					2	4790
1.475	4300					2.1	9980
1.5	8120					2.2	18000
1.6	49900					2.3	29000
1.7	138000					2.4	49600
1.8	275000					2.5	70800
1.9	473000						

Table 13. Respirable dust mass-based size distributions from APS

Midpoint aerodynamic diameter, d_a (μm)	$dM_{respir}/d\log_{10}(d_a)$ (mg m^{-3})							
	Fine		Medium		Coarse		Cutting	
	Avg	StDev	Avg	StDev	Avg	StDev	Avg	StDev
0.542	0.0202	0.0066	0.0199	0.0061	0.0310	0.0061	0.0224	0.0061
0.583	0.040	0.011	0.041	0.011	0.060	0.011	0.039	0.011
0.626	0.074	0.017	0.078	0.017	0.106	0.019	0.061	0.018
0.673	0.131	0.022	0.143	0.024	0.178	0.032	0.091	0.027
0.723	0.216	0.026	0.243	0.030	0.273	0.049	0.126	0.039
0.777	0.339	0.035	0.394	0.038	0.400	0.076	0.169	0.053
0.835	0.504	0.051	0.600	0.050	0.56	0.11	0.224	0.071
0.898	0.726	0.080	0.876	0.075	0.77	0.16	0.29	0.10
0.965	1.00	0.12	1.22	0.11	1.02	0.21	0.37	0.12
1.037	1.37	0.18	1.68	0.16	1.37	0.28	0.49	0.16
1.114	1.84	0.25	2.27	0.23	1.80	0.37	0.64	0.21
1.197	2.47	0.35	3.06	0.32	2.38	0.49	0.86	0.27
1.286	3.32	0.47	4.13	0.44	3.17	0.65	1.14	0.36
1.382	4.37	0.62	5.48	0.59	4.14	0.85	1.51	0.48
1.486	5.77	0.82	7.28	0.79	5.4	1.1	2.02	0.64
1.596	7.5	1.1	9.5	1.0	7.0	1.4	2.64	0.82
1.715	9.7	1.4	12.4	1.4	9.0	1.8	3.4	1.1
1.843	12.6	1.8	16.0	1.8	11.6	2.3	4.5	1.4
1.981	16.0	2.3	20.3	2.3	14.7	2.9	5.7	1.7
2.129	19.8	2.8	25.1	2.9	18.1	3.6	7.2	2.2
2.288	23.6	3.3	30.2	3.5	21.7	4.2	8.8	2.6
2.458	27.6	3.8	35.4	4.2	25.4	4.9	10.5	3.1
2.642	31.3	4.3	40.4	4.8	29.1	5.5	12.3	3.6
2.839	34.9	4.8	45.2	5.4	32.7	6.2	14.2	4.1
3.051	37.3	5.1	48.5	5.9	35.4	6.6	15.9	4.5
3.278	38.7	5.3	50.5	6.1	37.4	6.9	17.5	4.9
3.523	38.9	5.3	51.0	6.2	38.3	7.0	18.5	5.0
3.786	37.3	5.1	49.7	6.1	37.8	6.9	19.0	5.1
4.068	34.7	4.8	46.9	5.8	36.4	6.6	18.8	5.1
4.371	31.2	4.3	42.7	5.4	33.7	6.1	18.1	4.9
4.698	27.0	3.7	37.5	4.9	30.1	5.5	16.8	4.3
5.048	23.0	3.2	32.2	4.3	26.3	4.8	14.9	3.9
5.425	19.3	2.7	27.4	3.7	22.6	4.2	13.0	3.4
5.829	16.1	2.3	23.0	3.2	19.3	3.6	11.3	2.9
6.264	13.0	1.9	18.8	2.7	16.1	3.1	9.7	2.5
6.732	9.8	1.4	14.6	2.1	12.7	2.5	7.9	2.1
7.234	6.7	1.0	10.5	1.6	9.2	1.9	6.1	1.6
7.774	4.08	0.65	6.7	1.1	6.0	1.5	4.3	1.1
8.354	2.23	0.40	3.86	0.72	3.5	1.0	2.73	0.74
8.977	1.13	0.22	2.03	0.44	1.90	0.66	1.61	0.46
9.647	0.54	0.12	1.01	0.26	0.96	0.42	0.89	0.28
10.37	0.247	0.071	0.48	0.15	0.48	0.26	0.48	0.17
11.14	0.112	0.042	0.225	0.092	0.23	0.15	0.26	0.10
11.97	0.048	0.023	0.100	0.049	0.110	0.091	0.144	0.064
12.86	0.022	0.014	0.046	0.027	0.052	0.051	0.078	0.035
13.82	0.0094	0.0069	0.020	0.016	0.024	0.029	0.045	0.022
14.86	0.0039	0.0038	0.0086	0.0085	0.011	0.017	0.025	0.013
15.96	0.0017	0.0022	0.0038	0.0043	0.0051	0.0083	0.0141	0.0079
17.15	0.0006	0.0010	0.0016	0.0022	0.0022	0.0036	0.0082	0.0046
18.43	0.00025	0.00045	0.0007	0.0010	0.0010	0.0017	0.0046	0.0026
19.81	–	–	0.00013	0.00022	0.00018	0.00038	0.0022	0.0013

Appendix IV. Respirable Sample Dataset

Table 14. Complete dataset of respirable samples with corresponding stone mass removed during task and task duration

Disc	Run #	Sample #	Stone mass removed (g)	Task duration (min)	Dust mass (µg sample^{-1})	Dust LOD (µg sample^{-1})	Dust LOQ (µg sample^{-1})	Cristobalite mass (µg sample^{-1})	Cristobalite LOD (µg sample^{-1})	Cristobalite LOQ (µg sample^{-1})	Quartz mass (µg sample^{-1})	Quartz LOD (µg sample^{-1})	Quartz LOQ (µg sample^{-1})	Tridymite mass (µg sample^{-1})	Tridymite LOD (µg sample^{-1})	Tridymite LOQ (µg sample^{-1})
fine	1	S1	43	4	520	18	61	220	5	17	99	5	17	0	10	33
fine	1	S2	43	4	752	18	61	370	5	17	160	5	17	0	20	67
fine	1	S3	43	4	774	18	61	300	5	17	130	5	17	0	20	67
fine	1	S4	43	4	912	18	61	270	5	17	120	5	17	0	10	33
fine	1	T1	43	4	691	36	120	290	5	17	130	5	17	0	20	67
fine	1	T2	43	4	634	36	120	300	5	17	140	5	17	0	20	67
fine	1	T3	43	4	542	36	120	260	5	17	120	5	17	0	10	33
fine	1	T4	43	4	450	36	120	320	5	17	140	5	17	0	20	67
fine	2	S5	46	4	628	18	61	290	5	17	140	5	17	0	20	67
fine	2	S6	46	4	800	18	61	430	5	17	200	5	17	0	20	67
fine	2	S7	46	4	707	18	61	310	5	17	140	5	17	0	20	67
fine	2	S8	46	4	776	18	61	410	5	17	190	5	17	0	20	67
fine	2	T7	46	4	764	36	120	350	5	17	160	5	17	0	20	67
fine	2	T8	46	4	665	36	120	300	5	17	140	5	17	0	20	67
fine	2	T9	46	4	602	36	120	260	5	17	120	5	17	0	10	33
fine	2	T10	46	4	717	36	120	250	5	17	120	5	17	0	10	33
fine	3	S9	37	4	810	18	61	76	5	17	37	5	17	0	10	33
fine	3	S10	37	4	769	18	61	430	5	17	180	5	17	0	20	67
fine	3	S11	37	4	639	18	61	280	5	17	130	5	17	0	20	67
fine	3	S12	37	4	831	18	61	320	5	17	160	5	17	0	20	67
fine	3	T11	37	4	680	36	120	300	5	17	140	5	17	0	20	67
fine	3	T12	37	4	663	36	120	270	5	17	130	5	17	0	20	67
fine	3	T13	37	4	574	36	120	300	5	17	130	5	17	0	10	33
fine	3	T14	37	4	715	36	120	300	5	17	140	5	17	0	20	67
medium	4	S13	63	4	700	18	61	350	5	17	150	5	17	0	20	67
medium	4	S14	63	4	1340	18	61	470	5	17	210	5	17	0	20	67
medium	4	S15	63	4	1002	18	61	320	5	17	140	5	17	0	20	67
medium	4	S16	63	4	867	18	61	400	5	17	180	5	17	0	20	67
medium	4	T15	63	4	851	36	120	400	5	17	180	5	17	0	20	67

medium	4	T16	63	4	718	36	120	220	5	17	95	5	17	0	10	33
medium	4	T17	63	4	663	36	120	320	5	17	140	5	17	0	20	67
medium	4	T18	63	4	816	36	120	380	5	17	170	5	17	0	20	67
medium	5	S17	67	4	657	18	61	350	5	17	160	5	17	0	20	67
medium	5	S18	67	4	1003	18	61	450	5	17	200	5	17	0	20	67
medium	5	S19	67	4	701	18	61	330	5	17	150	5	17	0	20	67
medium	5	S20	67	4	986	18	61	510	5	17	220	5	17	0	20	67
medium	5	T19	67	4	921	36	120	410	5	17	190	5	17	0	20	67
medium	5	T20	67	4	762	36	120	370	5	17	170	5	17	0	20	67
medium	5	T21	67	4	728	36	120	380	5	17	160	5	17	0	20	67
medium	5	T22	67	4	914	36	120	460	5	17	210	5	17	0	20	67
medium	6	S21	62	4	806	18	61	340	5	17	150	5	17	0	20	67
medium	6	S22	62	4	934	18	61	470	5	17	210	5	17	0	20	67
medium	6	S23	62	4	732	18	61	290	5	17	130	5	17	0	20	67
medium	6	S24	62	4	963	18	61	460	5	17	200	5	17	0	20	67
medium	6	T23	62	4	907	36	120	440	5	17	210	5	17	0	20	67
medium	6	T24	62	4	718	36	120	330	5	17	150	5	17	0	20	67
medium	6	T25	62	4	665	36	120	330	5	17	150	5	17	0	20	67
medium	6	T26	62	4	909	36	120	410	5	17	190	5	17	0	20	67
coarse	7	S25	78	4	536	18	61	240	5	17	100	5	17	0	10	33
coarse	7	S26	78	4	843	18	61	420	5	17	180	5	17	0	20	67
coarse	7	S27	78	4	547	18	61	280	5	17	120	5	17	0	10	33
coarse	7	S28	78	4	751	18	61	370	5	17	170	5	17	0	20	67
coarse	7	T29	78	4	796	36	120	360	5	17	170	5	17	0	20	67
coarse	7	T30	78	4	572	36	120	260	5	17	120	5	17	0	10	33
coarse	7	T31	78	4	553	36	120	240	5	17	110	5	17	0	10	33
coarse	7	T32	78	4	772	36	120	380	5	17	170	5	17	0	20	67
coarse	8	S29	71	4	510	18	61	240	5	17	110	5	17	0	10	33
coarse	8	S30	71	4	851	18	61	390	5	17	170	5	17	0	20	67
coarse	8	S31	71	4	786	18	61	260	5	17	120	5	17	0	20	67
coarse	8	S32	71	4	1044	18	61	380	5	17	180	5	17	0	20	67
coarse	8	T33	71	4	770	36	120	360	5	17	170	5	17	0	20	67
coarse	8	T34	71	4	584	36	120	240	5	17	120	5	17	0	20	67
coarse	8	T35	71	4	531	36	120	270	5	17	120	5	17	0	10	33
coarse	8	T36	71	4	770	36	120	340	5	17	160	5	17	0	20	67
coarse	9	S33	83	4	582	18	61	270	5	17	120	5	17	0	20	67
coarse	9	S34	83	4	870	18	61	490	5	17	210	5	17	0	20	67
coarse	9	S35	83	4	569	18	61	260	5	17	120	5	17	0	20	67
coarse	9	S36	83	4	840	18	61	420	5	17	190	5	17	0	20	67
coarse	9	T37	83	4	792	36	120	380	5	17	180	5	17	0	20	67
coarse	9	T38	83	4	551	36	120	280	5	17	130	5	17	0	20	67
coarse	9	T39	83	4	546	36	120	300	5	17	130	5	17	0	20	67

coarse	9	T40	83	4	776	36	120	430	5	17	190	5	17	0	20	67
cutting	11	S43	29	2.5[a]	156	18	61	89	5	17	38	5	17	0	10	33
cutting	11	S44	29	2.5[a]	326	18	61	160	5	17	68	5	17	0	10	33
cutting	11	S45	29	2.5[a]	198	18	61	74	5	17	33	5	17	0	10	33
cutting	11	S46	29	2.5[a]	325	18	61	130	5	17	56	5	17	0	10	33
cutting	11	T43	29	2.5[a]	253	36	120	120	5	17	51	5	17	0	10	33
cutting	11	T44	29	2.5[a]	178	36	120	87	5	17	38	5	17	0	10	33
cutting	11	T45	29	2.5[a]	151	36	120	69	5	17	28	5	17	0	10	33
cutting	11	T46	29	2.5[a]	253	36	120	110	5	17	45	5	17	0	10	33
cutting	12	S47	34	2.5[a]	164	18	61	66	5	17	27	5	17	0	10	33
cutting	12	S48	34	2.5[a]	267	18	61	97	5	17	41	5	17	0	10	33
cutting	12	S49	34	2.5[a]	255	18	61	63	5	17	26	5	17	0	10	33
cutting	12	S50	34	2.5[a]	300	18	61	110	5	17	44	5	17	0	10	33
cutting	12	T47	34	2.5[a]	221	36	120	100	5	17	43	5	17	0	10	33
cutting	12	T48	34	2.5[a]	153	36	120	79	5	17	31	5	17	0	10	33
cutting	12	T49	34	2.5[a]	139	36	120	76	5	17	27	5	17	0	10	33
cutting	12	T50	34	2.5[a]	233	36	120	96	5	17	44	5	17	0	10	33
cutting	13	S51	51	4[a]	212	18	61	89	5	17	35	5	17	0	10	33
cutting	13	S52	51	4[a]	395	18	61	160	5	17	73	5	17	0	10	33
cutting	13	S53	51	4[a]	213	18	61	100	5	17	40	5	17	0	10	33
cutting	13	S54	51	4[a]	301	18	61	130	5	17	54	5	17	0	10	33
cutting	13	T51	51	4[a]	338	36	120	160	5	17	74	5	17	0	10	33
cutting	13	T52	51	4[a]	225	36	120	100	5	17	43	5	17	0	10	33
cutting	13	T53	51	4[a]	216	36	120	110	5	17	46	5	17	0	10	33
cutting	13	T54	51	4[a]	327	36	120	160	5	17	63	5	17	0	10	33

[a]estimated task duration

Delivering on the Nation's promise:

Promoting productive workplaces through safety and health research

Get More Information

Find NIOSH products and get answers to workplace safety and health questions:

1-800-CDC-INFO (1-800-232-4636) | TTY: 1-888-232-6348
CDC/NIOSH INFO: cdc.gov/info | cdc.gov/niosh
Monthly *NIOSH eNews*: cdc.gov/niosh/eNews